NOAA Technical Report ERL 331-APCL 34

U.S. DEPARTMENT OF COMMERCE
NATIONAL OCEANIC AND ATMOSPHERIC ADMINISTRATION
Environmental Research Laboratories

Airborne Infrared Imagery of Arctic Sea Ice Thickness

P. M. KUHN

L. P. STEARNS

R. O. RAMSEIER

ULDER, COLO.
Y 1975

U.S. DEPARTMENT OF COMMERCE
Rogers C. B. Morton, Secretary

NATIONAL OCEANIC AND ATMOSPHERIC ADMINISTRATION
Robert M. White, Administrator
ENVIRONMENTAL RESEARCH LABORATORIES
Wilmot N. Hess, Director

NOAA TECHNICAL REPORT ERL 331-APCL 34

Airborne Infrared Imagery of Arctic Sea Ice Thickness

P. M. KUHN

L. P. STEARNS

R. O. RAMSEIER

BOULDER, COLO.
May 1975

For sale by the Superintendent of Documents, U. S. Government Printing Office, Washington, D. C. 20402

NOTICE

The Environmental Research Laboratories do not approve, recommend, or endorse any proprietary product or proprietary material mentioned in this publication. No reference shall be made to the Environmental Research Laboratories or to this publication furnished by the Environmental Research Laboratories in any advertising or sales promotion which would indicate or imply that the Environmental Research Laboratories approve, recommend, or endorse any proprietary product or proprietary material mentioned herein, or which has as its purpose an intent to cause directly or indirectly the advertised product to be used or purchased because of this Environmental Research Laboratories publication.

CONTENTS

FIGURES

TABLES

COLOR PLATES

AIRBORNE INFRARED IMAGERY OF ARCTIC SEA ICE THICKNESS

P. M. Kuhn, L. P. Stearns, and R. O. Ramseier[1]

The paper presents an empirically observed correlation between ice thickness and infrared brightness ice temperature, based on heat transfer and heat flux at the sea-ice and sea-air interfaces. During the February-March 1973 NASA-USSR Bering Sea Ice Experiment (BESEX), simultaneous surface coring data were combined with infrared imagery in the 840-1237 cm^{-1} spectral band, acquired from the NASA Convair 990 Jet Laboratory. From the combined data, we inferred ice thicknesses from ±5 cm for thin ice to ±17 cm for thick ice. Coldest sea ice temperatures during BESEX, approximately -22 to -24C, occurred at the tops of the pressure ridges, exhibiting a singular vein-like structure clearly discernible in the highly detailed color enhanced imagery. Freshly refrozen leads and polynyas exhibited the highest brightness temperatures, averaging -3.0 and -0.5C respectively.

1. INTRODUCTION

Research results from the BESEX expedition over the Arctic Ocean and Bering Sea in February and March 1973 indicated that infrared (IR) thermal emission from sea ice varies significantly with ice thickness. The ice thickness is inversely proportional to the radiant emission and convective heat transfer at the surface, and directly proportional to the difference between ice surface temperature and the sea temperature at the base of the ice layer.

An areal presentation of sea ice thickness, as determined by high speed airborne IR imagery, can be applied in several important ways. For example, with such a presentation ice thickness can be estimated as a function of time. Questions on rates of freeze and thaw associated

[1]Department of the Environment, Ottawa, Ontario, Canada.

with ice thickness can be resolved for shipping and sub-surface marine activities. Insight can be acquired into the thermodynamics of the rates of ice formation and dissipation, a key consideration in the theoretical basis of this study. Our research uses the areal presentations to develop a usable relationship between IR remotely sensed ice thermal emission and sea ice thickness.

Sea ice brightness temperatures converted to physical ice temperatures were related to simultaneous surface corings of ice thickness. The IR imagery was false color enhanced by amplitude-slicing techniques to highlight the ice thickness pattern. The physical temperature of ice is obtained by "calibrating" the atmosphere during ascent and descent.

NASA's Convair 990 Jet Laboratory supporting the research efforts carried an IR line scanning mapper during the 1972 and 1973 experiments. Flight operations over the ice were conducted at elevations ranging from 300 m to 11.5 km. Due to frequent (50% of the time) interspersion of cirriform clouds between flight level and the surface, the 11.5 km altitude did not yield as good IR imagery as did the 3.3 km and 300 m altitudes. However, uniform cirrus coverage allowed good imagery ice thickness inferences from 10 km. The 3.3 km altitude with its wide scan track, 6.6 km, furnished excellent false color enhanced imagery with a spatial, elemental resolution of approximately 2.0 m. The adjustment of the brightness temperature of the ice to obtain the physical temperature is approximately +1.5C at 3.3 km and +4.0C at 11.5 km in the 840-1237 cm^{-1} window channel employed.

2. INFRARED MAPPING SYSTEM

The infrared mapper is a passive, airborne imaging system employing an LN cooled Hg-Cd-Te detector (Texas Instruments, RS-310-C) that scans the interface below, along, and out to 45° to either side of nadir of the flight track. In so doing, it produces a continuous image of the surface beneath.

True angle rectification is always maintained by gyro roll-stabilization. Inflight calibration is achieved without sacrifice of lateral imagery coverage by a "blackbody" dual temperature monitored sliding door aperture (fig. 1). The system was installed in the engineering and electronics hold area of the NASA Convair 990 jet, immediately to the rear of the nose-wheel well. A small boundary layer fence, visible in the illustration, eliminated any resonance effects in the cavity. The complete scanner system was sealed to the jet hull via a pressure bulkhead.

Figure 1. Convair 990 aircraft installation for infrared imager.

Figure 2 shows the system with thermal ribbon heaters installed along the walls of the cavity to permit the compartment operating temperature to be monitored and controlled within the cabin. The imager specifications are summarized in Table 1.

3. ICE THICKNESS AND HEAT TRANSFER AT THE ICE-AIR INTERFACE

By assuming an equilibrium among the heat conducted from water through ice to the air-ice interface, the net radiant heat exchange at this interface, and the heat convection at the ice to the surface, it is theoretically possible to determine ice thickness on water by areal infrared imagery of the ice interface temperature. A critical problem in an equilibrium hypothesis for calculating ice thickness from observation encompassing the ice-air interface power budget is the varying snow cover on the ice. A large scale mean ice thickness of a variously snow-

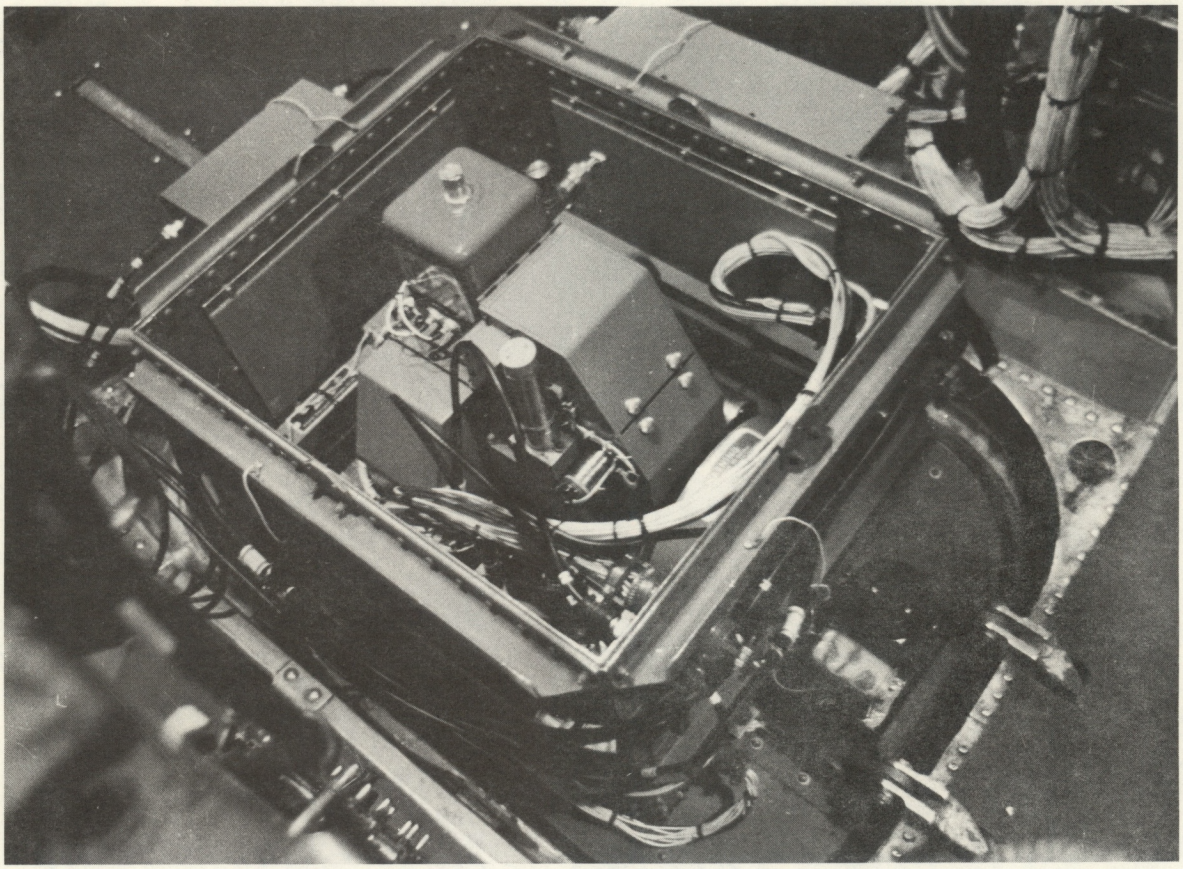

Figure 2. Pressure bulkhead imager installation, Convair 990

covered ice surface is obtained. Finally theoretical curves of various ice thicknesses are generated as functions of differing ice temperatures and ambient air temperatures. Subsequently, some of the variables in the power budget equation at the ice-air interface are adjusted to minimize the r.m.s. difference between observed and radiometrically inferred ice thicknesses.

It is important to consider net radiant heat flux (the difference between the upward directed and downward directed hemispheric flux), not just the upward radiant flux, in this relationship. Further it is necessary to treat the physical model mathematically for the mean cofficient of heat transfer by convection. Le Schack [1974] and Gloersen et al. [1974] present simple models of a relationship between heat transfer equilibrium and ice thickness. The present study, however, uses a different approach to heat transfer by thermal radiation and by convection.

Table 1. Imager Specifications.

Imager	Specifications
Resolution (milliradians)	1.0 x 1.0 5.0 x 5.0
Field of view (degrees)	90
V/H range (radians/second)	0.02 to 0.35
Scanner RPM	3000 (200 scans/second)
Noise equivalent temperature change (N.E. Δt) with LN_2 cooled detector	0.15C
Wave length region (cm^{-1})	840-1237 1800-3000

The continuity of heat flux across the air-ice interface is the premise in the analysis of the relationship of forced convection, net radiation and conduction, and ice thickness. Experimentally the relationship appears plausible and demonstrates a respectable accuracy. The surface temperature of the ice is determined by its thickness, by the constant water temperature at the base of the ice layer, and by the "constant" air temperature at approximately 1.6 m above the ice surface.

From preliminary calculations the dominant terms in the heat balance at the ice-air interface are the one dimensional heat conduction through the ice, S, and the forced convective heat transfer, H. Latent heat effects, E, are estimated to be at least an order of magnitude less than S and H. (Table 2 lists the symbols used in the text.) Defining the heat conduction through the ice by

$$S = K_{ice} \frac{\Delta T}{\Delta z}_{ice}, \qquad (1)$$

where $K_{ice} = a + b\bar{T}_{ice}$, we may express the ice thickness in terms of conduction, convection, and sensible heat flux as

Table 2. Symbols.

B	Planck function (cal cm^{-1} sr^{-1} sec^{-1})
C_θ	Heat transfer coefficient (dimensionless)
E	Latent heat (cal cm^{-2} sec^{-1})
F_D	Infrared downward irradiance or flux (cal cm^{-2} sec^{-1})
F_N	Infrared net irradiance (cal cm^{-2} sec^{-1})
F_U	Infrared upward irradiance or flux (cal cm^{-2} sec^{-1})
F_{NT}	Net total (IR and solar) radiation at ice surface (cal cm^{-2} sec^{-1})
G	Function of the heat-transfer coefficient
H	Forced convective heat transfer (cal cm^{-2} sec^{-1})
K_{ice}	Thermal conductivity for ice (cal deg^{-1} cm^{-1} sec^{-1})
L	Monin-Obukhov length (cm)
N	Radiance (cal cm^{-2} sr^{-1})
R	Reflection or scatter
Ri	Richardson number
S	Heat conduction through ice to the surface (cal cm^{-2} sec^{-1})
S_c	Solar constant (cal cm^{-2} sec^{-1})
S_D	Solar downward irradiance or flux (cal cm^{-2} sec^{-1})
S_U	Solar upward irradiance or flux (cal cm^{-2} sec^{-1})
T	Temperature
T_{ice}	Ice temperature (K)
ΔT	Sea temperature minus air temperature (K)
ΔX	Optical mass (cm)
a	Constant = 0.008443
b	Constant = -0.0000133
c_p	Specific heat of air (cal gm^{-1} deg^{-1})
g	Acceleration of gravity = 980 cm sec^{-2}
k	von Karman's constant = 0.35
p	Pressure (millibars)
u	Wind, velocity (cm sec^{-1})
z_{ice}	Ice thickness (cm)
$(z_r-z_o)/L$	Obukhov stability parameter
α	Angle
θ	Potential temperature (K)
$\overline{\theta}$	Average of air and ice temperature (K)
$\Delta\theta$	Ice temperature minus air temperature (K)
ν	Wave number frequency (cm^{-1})
ρ	Air density (g cm^{-3})
σ	Total extinction coefficient (cm^{-1})
τ	Infrared transmission
τ_s	Solar transmission

Subscripts

r	Reference level
o	Ice level
H_2O	Water
CO_2	Carbon dioxide
O_3	Ozone

$$\Delta z_{ice} = \frac{K_{ice}\Delta T_{ice}}{F_{NT} - H} . \qquad (2)$$

As stated, it was found from a consideration of the relative values of the various terms of the heat balance that forced heat transfer is a major contributing term in the determination of the ice thickness. Since we are attempting to explain why IR surface imagery does allow ice thickness determination, a brief review of calculation methods for the estimation of forced convective heat flux is in order.

4. CONVECTIVE HEAT FLUX

The procedure to be followed in convective heat flux calculation involves three steps:

a. Determine the Richardson number (Ri) which is a measure of the stability of the surface air layer. This parameter is determined from observations of the air-ice temperature difference at the reference level above the ice and of the wind speed at the reference level. Thus,

$$Ri = \frac{g\Delta\theta(z_r - z_o)}{\bar{\theta}u^2} \tag{3}$$

The reference level is assumed to be 160 cm. Near the surface the potential temperature, θ, and air temperature, T, are virtually identical.

During the ice verification missions to be described, air temperatures and winds at 160 cm, z_r, were obtained by ground observers. The reference level temperature and wind at z_r may be determined by extrapolation downward from a very low-level (15 m) aircraft pass. Temperatures are observed with a horizontal-looking IR CO_2 band air temperature radiometer; winds are determined from the aircraft inertial navigation system. Climatological means and variances could be used in assessing the reference level temperature and wind speed.

b. Determine the convective heat transfer coefficient, C_θ, as a function of the Richardson number after Deardorff [1972] and Nickerson and Smiley [1975]. They develop another form of the Richardson number,

$$Ri = \frac{(z_r - z_o)G}{kLF^2}, \tag{4}$$

to make possible a determination of C_θ as a function of Ri, observed. They show F, a function of the friction coefficient, and G, a function of the heat transfer coefficient, related to C_θ by

$$C_\theta = \frac{1}{FG}. \tag{5}$$

Table 3, solutions of (4) and (5), provides values of C_θ as a function of Ri. The calculation of the surface heat flux may then be expressed by

$$H = C_\theta \rho c_p \Delta\theta u. \qquad (6)$$

Table 3. Solutions of Equations (4) and (5).

$(z_r - z_o)/L$	Ri	C_θ
.0000	.000000	.000000
.0010	.000069	.001437
-.0100	-.000691	.001448
-.0200	-.001386	.001459
-.0300	-.002084	.001468
-.0400	-.002784	.001477
-.0500	-.003486	.001486
-.0600	-.004190	.001494
-.0700	-.004896	.001502
-.0800	-.005603	.001510
-.0900	-.006312	.001517
-.1000	-.007023	.001524
-.1100	-.007735	.001531
-.1200	-.008448	.001538
-.1300	-.009162	.001544
-.1400	-.009878	.001551
-.1500	-.010594	.001557
-.1600	-.011312	.001563
-.1700	-.012031	.001569
-.1800	-.012750	.001574
-.1900	-.013471	.001580
-.2000	-.014192	.001585
-.3000	-.021450	.001634
-.4000	-.028776	.001676
-.5000	-.036156	.001713

The 160-cm level wind speed was obtained from surface observations during coring or from climatological estimates based on the geostrophic wind. The aircraft-observed wind speed was also extrapolated down to the 1.6-m level as a further check. Wind speeds averaged 500 cm sec^{-1} by all methods.

c. The total net radiant flux at the surface is given by

$$F_{NT} = F_D - F_U + S_D - S_U. \tag{7}$$

The infrared radiance is calculated from

$$N = -\int_{\nu}\int_{p} B(\nu,T(p)\ldots)\ \frac{\partial\tau}{\partial p}\, dp d\nu - \int_{\nu} B(\nu,T(p_o)\ \tau_o)\ d\nu\ . \tag{8}$$

In (8) the upward infrared transfer involves a solution of both right hand integrals while the downward infrared transfer requires only solution of the first integral. The multiplicity theorem permits us to define $d\tau$ for determining N in (8) by

$$1.0 - \tau_{H_2O} * \tau_{CO_2} * \tau_{O_3} * \tau_{continuum} = d\tau. \tag{9}$$

The infrared irradiance or flux (cal cm^{-2} sec^{-1}) is given by

$$F_N = 2\pi \int_0^{\pi/2} N(\alpha)\ \sin\alpha\ \cos\alpha\ d\alpha \tag{10}$$

The solar radiation (downward and upward directed) may be calculated for a fixed frequency interval from the expressions

$$S_D = S_C * \tau_s * e^{-\sigma \Delta X\ \sec\zeta\ \cos\zeta} \tag{11}$$

and

$$S_U = RS_D. \tag{12}$$

Further, observations at T-3 with the Suomi-Kuhn radiometersonde [1958], as late as 1971, provide an excellent average for the surface total net radiation. For the period 15 February through 14 March this average from observation and eq. (7) is 0.00016 cal cm^{-2} sec^{-1}.

For a typical March Bering Sea situation at 1200 hours sun time under cloudless conditions, the surface heat flux is calculated by

$$F_{NT} = S + H + E$$

where $F_{NT} = 0.00016$ cal cm^{-2} sec^{-1},

$S = +0.001738$ cal cm^{-2} sec^{-1},

$H = -0.001563$ cal cm^{-2} sec^{-1},

and $E = 0.00002$ cal cm^{-2} sec^{-1}.

5. OBSERVED COLOR ENHANCED IR IMAGERY AND CALCULATED ICE THICKNESS

False color imagery enhancement is obtained either by photographic or magnetic tape analog signal input to an analog-to-digital quantizing system. This device, accepting either TV camera monitored gray scale film imagery or analog magnetic tape input, permits assignment of up to twelve colors to gray scale "steps" existing in the data input. The output of the quantizer, the heart of the false color enhancement, may be either digital data or color imagery on a color TV monitor. The latter is perhaps the most common output and was employed in this study. Color temperature calibration is facilitated by the linear nature of radiant emission from a blackbody between 273K and 250K and by the linearity of the gray scale film density. A further aid to color calibration exists in the constant flight presence of a nadir-looking, fixed-field radiometer with ± 0.1C relative accuracy, always augmenting the nadir temperature of the imagery.

Ice thicknesses were verified at the surface for nine imagery overpasses during BESEX. The imagery on a diagonal track from 62.38°N latitude by 177.25°W longitude to 61.44°N latitude by 175.25°W longitude during the mission of 5 March 1973 at a flight altitude of approximately 300 m appears in color plate No. 1. Sites A5, A2, and A3G are marked.

The curves of ice thickness (ordinate) versus ice temperature (abscissa) for various air temperature regimes, calculated from eqs. (2) through (7), are displayed in figure 3. The plotted points of Figure 4, representing calculated ice thicknesses vs observed ice thicknesses are listed in Table 4. The r.m.s. difference between calculated and observed thicknesses for this data set is 10.0 cm. Best agreement occurs for thickness less than 40 cm.

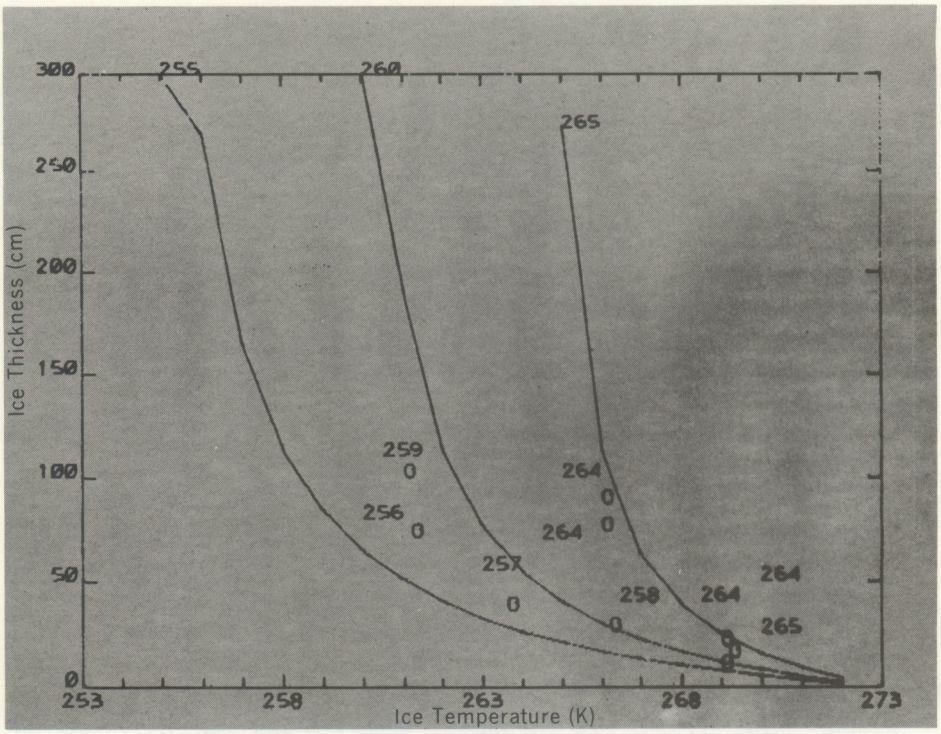

Figure 3. Ice thickness as a function of ice temperature and air temperature.

Plate 2 is a false color IR montage of the 1972 AIDJEX site acquired at 3.3 km during the 3 March 1973 mission. The areal extent is from 76.8°N to 77.8°N by 153.4°W to 154.1°W, roughly 12 km by 96 km. This mid-altitude false color imagery is color coded from -2 to -24C and represents approximately one hour's flight time. Features as narrow as 3 m are visible. They are too numerous to cover in detail and we identify only three, namely, pressure ridges, thick ice, and re-frozen thin polynyas.

With Plate 2, it is possible to follow the steps of estimating from an IR color montage the ice thickness for three indicated areas.

The medium blue represents -17C to -19C relatively thick ice between pressure ridges. The air temperature extrapolated to 2 m from the IR free air temperature radiometer for the same areas would be approximately -19C.

The inferred ice thickness for the medium blue in the plate would be in excess of 1.0 m. The medium blue areas were typical of the AIDJEX camp site in an area of reported multi-year and first year ice from the microwave radiometer signatures.

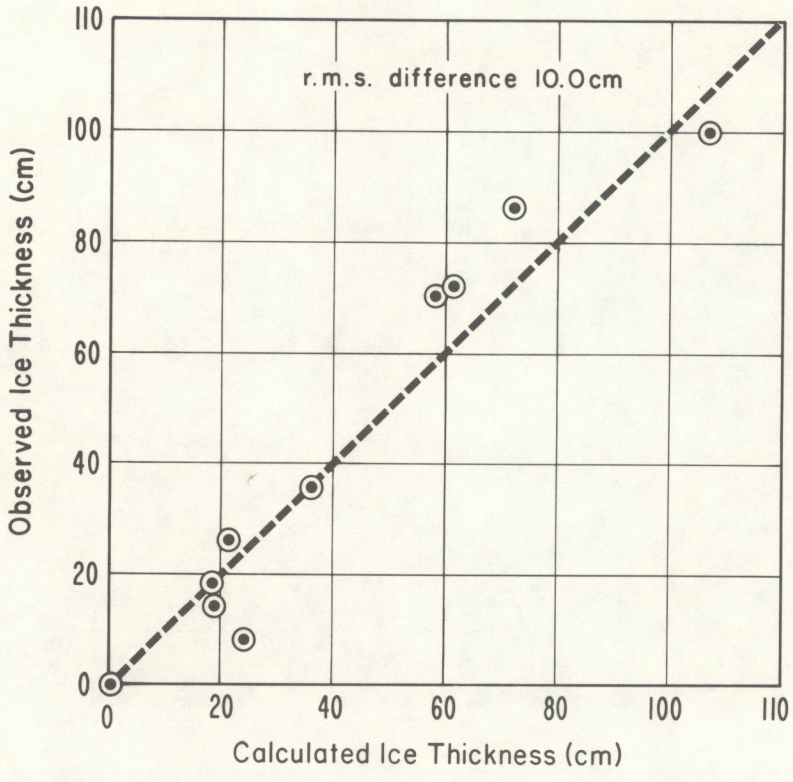

Figure 4. Calculated and observed ice thickness scattergram.

The coldest IR brightness temperatures scanned during this run, appearing as pinks and considerable veins of very dark blue or black, were those of the tops of compression ridges at -22C to -24C. The vein-like structure of the compression ridges, some 1.20 to 1.80 meters high, is very clear. That they are insulated from the ice surface accounts for their colder temperatures with an inferred thickness in excess of 2 m. The bright red, yellow, and black areas are the thermal imagery of freshly frozen leads up to 40 km long. The warmest temperatures averaged approximately -2C. From figure 3 it can be inferred that the ice thickness does not exceed 8 cm.

Comments by the ice observer aboard the aircraft such as "Grease ice on lead just passed," aided in the verification as did analyses of ice corings near the AIDJEX camp [Meeks et al. 1973] that indicated the camp to be"... located on thick multi-year ice." [Gloersen et al., 1973].

Plate 3 illustrates nearly open polynyas and pancake ice in false color and makes possible an infrared inference of ice thicknesses from the curves of figure 3. The inferred air temperature was 260K. From these data, the red to black areas would be open water to "grease" ice.

Table 4. Observed Ice Thickness, Calculated Ice Thickness, and Ice Temperature.

Site	Date	T_{ice} (K)	T_{air} (K)	Observed Thickness	Snow Cover	Calculated Thickness
M1	2-20-73	261.0	258.6	100	4.5	107
NW5G	2-28-73	269.2	265.2	8	0	24
SE4G	2-29-73	269.2	264.2	19	0	19
SE0	2-29-73	266.2	264.2	87	7	72
SE1	2-29-73	266.2	263.7	74	6	61
SE1G	2-29-73	269.2	263.7	14	0	18
*A5	3- 5-73	261.2	256.2	71	9.5	58
*A2	3- 5-73	263.6	257.2	36	1.5	36
*A3G	3- 5-73	266.2	258.2	26	0	21
*Lead2	3- 5-73	269.0	253.0	Lead	0	6
*Lead3	3- 5-73	265.0	253.0	Lead	0	17

*See Plate 1.

On the other hand, the blue pancake ice at a temperature 261K would have a thickness in excess of 1.4 meters. Both are reasonable conclusions; pancake ice in the area, but not at the same locale, was estimated to be from 1.5 to 2.0 meters thick. The red areas indicate refrozen leads at a temperature of -2 to -3C, with thickness inferred to be less than 10 cm (fig. 3).

6. CONCLUSIONS

Assuming an equilibrium among ice heat conduction, net total radiant heat exchange, and heat convection at the ice-air or ice plus snow-air interface, we can calculate ice thickness from remote airborne imagery of the surface temperature. Solar and net total radiometers aboard the CV-990, measuring the upper and lower hemisphere total (solar and IR) radiation, as well as aircraft to surface wind speed extrapolations, provided estimates of the net total radiation and forced heat convection.

Calculations of the ice thickness based on heat transfer equilibrium agreed very well with surface observations of the ice thickness, resulting in an r.m.s. difference between calculation and observation of approximately 10.0 cm. This significant result from airborne IR imagery was undoubtedly enhanced by the generally very light snow cover, averaging 3.0 cm over the test areas.

Infrared areal presentations provide a fast convenient means of estimating ice thickness. The technique described can provide, with photographic clarity, continuous areal surveys of ice thickness, freeze and thaw regions, and rates of ice formation and dissipation. It also appears possible to alter, in calculations, the values of ice thermal conductivity to include those of an upper snow layer, although the very light snow cover during these Bering Sea overflights precluded testing such a modification. This and more verification are in order for the 1975 AIDJEX (Arctic Ice Dynamics Joint Experiment) expedition.

7. REFERENCES

Deardorff, J. W. (1972): Parameterization of the planetary boundary layer for use in general circulation models, *Monthly Weather Review*, 100(2), 93-106.

Gloersen, P., R. Ramseier, W. J. Campbell, P. M. Kuhn and W. J. Webster, Jr. (1974): Ice thickness distribution as inferred from infrared and remote sensing during the Bering Sea Experiment, Chapter 4, X-910-74-14, report revised June 1974, Goddard Space Flight Center, 193 pp.

Gloersen, P., W. Nordberg, T. S. Schmugge, T. T. Wilheit and W. J. Campbell (1973): Microwave signatures of first year and multi-year ice, *J. Geophys. Res.*, 78(18), 3564-3572.

Le Schack, Leonard A. (1974): Potential use of satellite IR data for ice thickness mapping in *The coast and shelf of the Beaufort Sea* (Symposium on Beaufort Sea Coast and Shelf Research, San Francisco, CA, January 7-9), 1974, Arctic Institute of North America, p. 243-267.

Meeks, D. C., R. E. Ramseier and W. J. Campbell (1975): A study of microwave emission properties of sea ice - AIDJEX 1972, *J. of Remote Sensing* (accepted for publication).

Nickerson, E. C. and V. E. Smiley (1975): Surface layer and energy budget parameterizations for mesoscale models, *J. Appl. Meteor.* 14, 297-300 (Correction to appear in *J. Appl. Meteor.*, August 1975.)

Suomi, V. E. and P. M. Kuhn (1958): An economical net radiometer, *Tellus*, 10(1), 160-163.

Besex 12
Diagonal
5 Mar. 1973

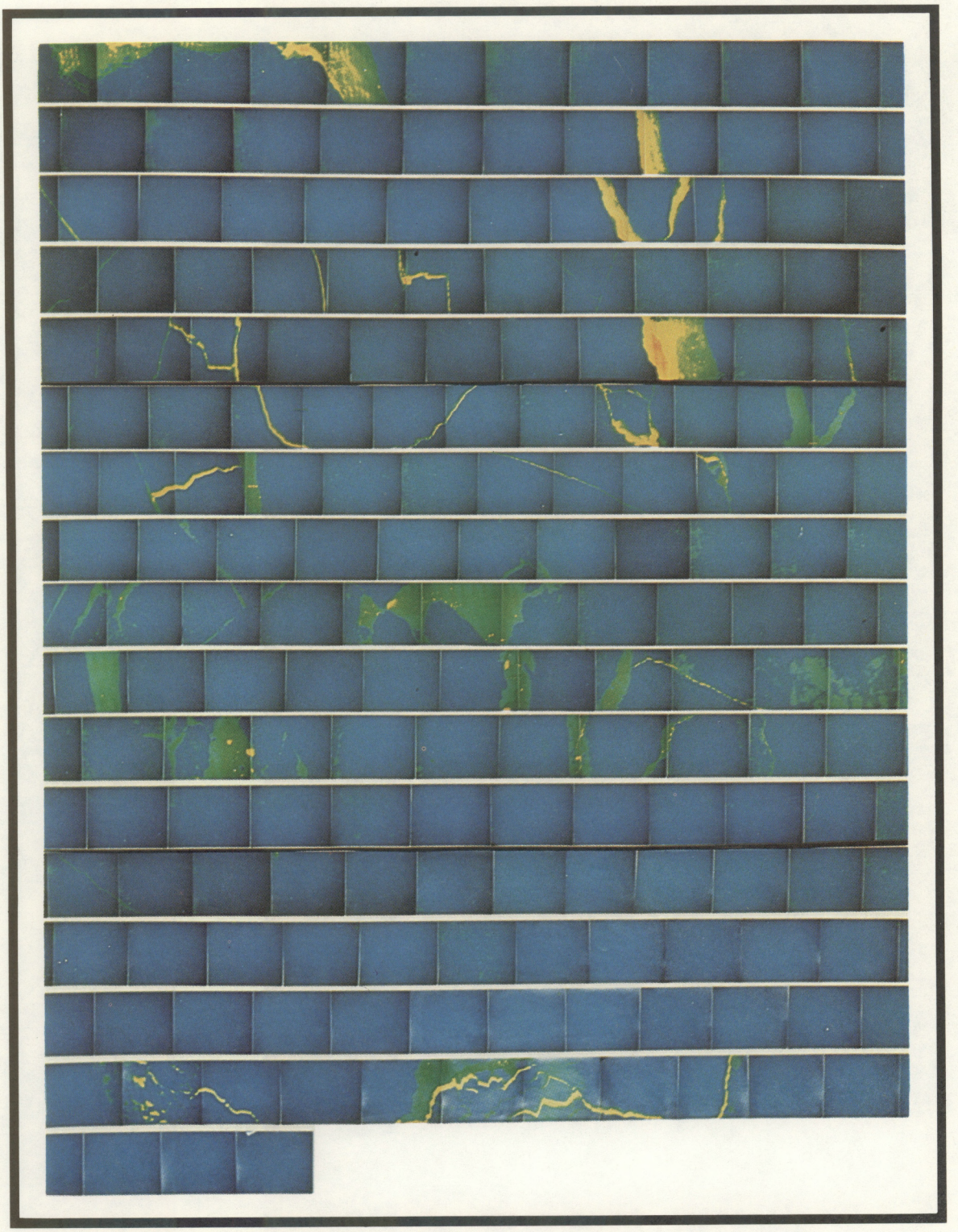

Plate 1. BESEX 12 (5 March 1973) 1000 foot diagonal.

Besex 11
Bering Sea
Alt. 10000ft.
March 3, 1973

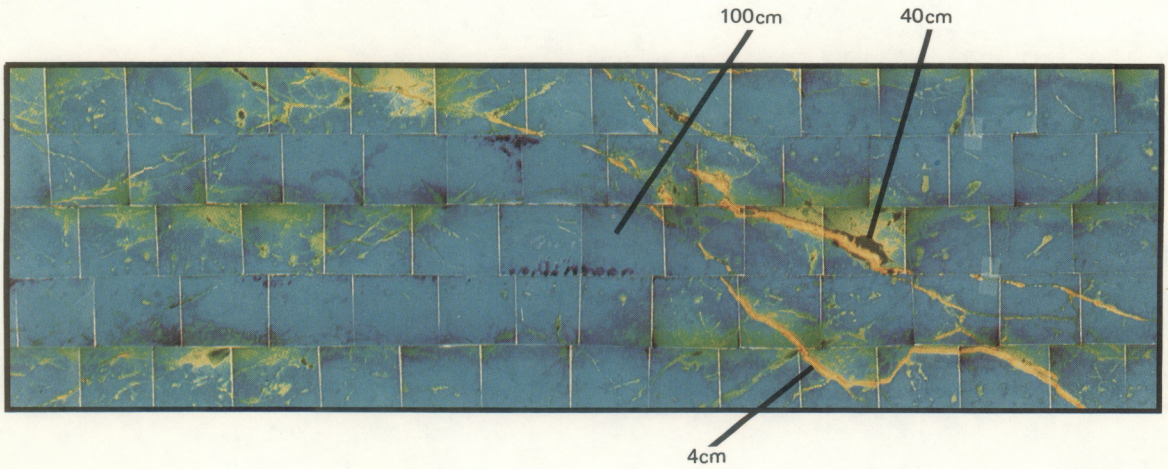

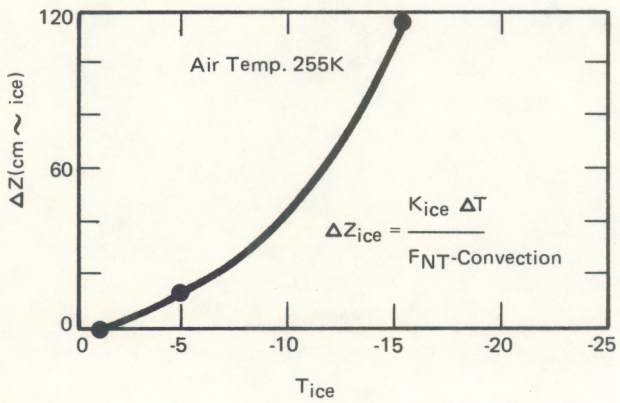

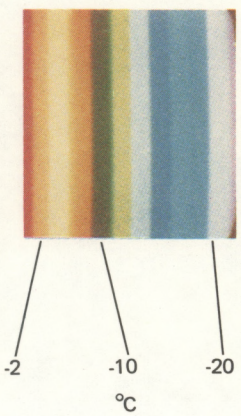

Plate 2. BESEX 11 (3 March 1973) 10,0000 foot montage.

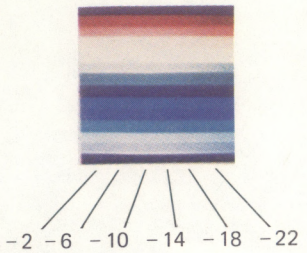

Besex 5

Bering Sea Feb. 20, 1973

Pressure altitude = 965 ft.
Radar altitude = 502 ft.

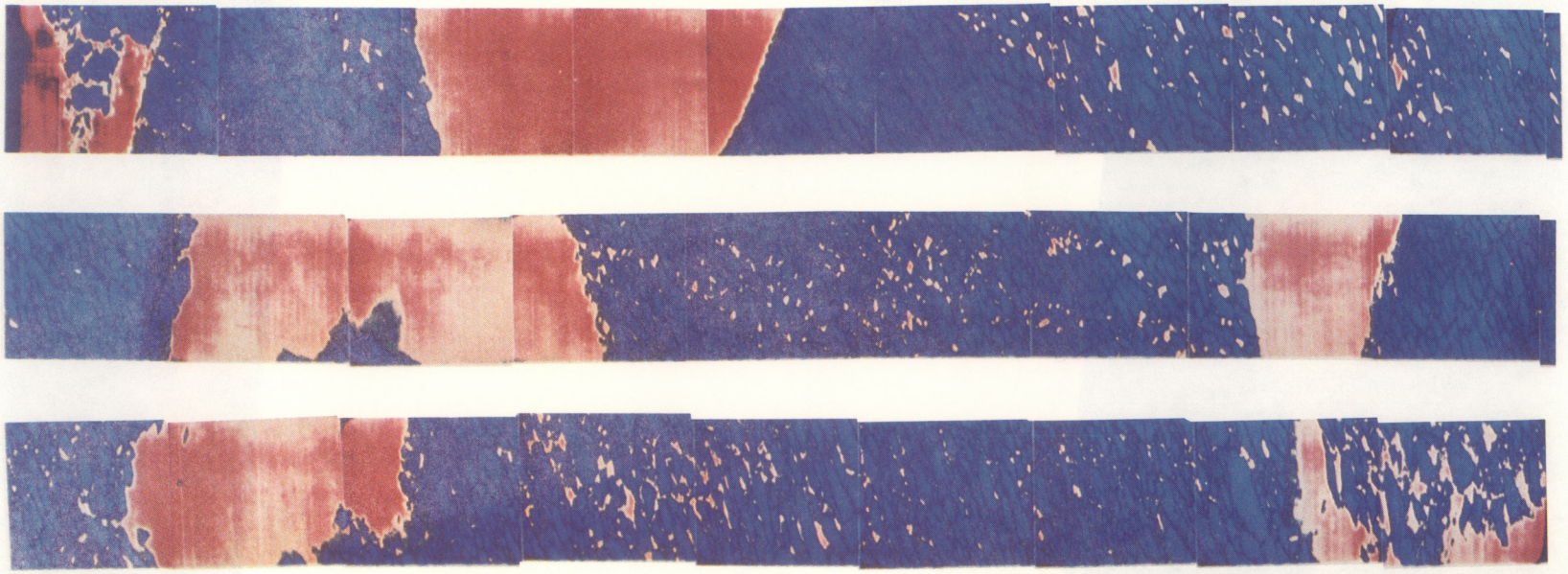

Plate 3. BESEX 5 (20 February 1973) 1000 foot diagonal.

ENVIRONMENTAL RESEARCH LABORATORIES

The mission of the Environmental Reasearch Laboratories is to study the oceans, inland waters, the lower and upper atmosphere, the space environment, and the earth, in search of the understanding needed to provide more useful services in improving man's prospects for survival as influenced by the physical environment. Laboratories contributing to these studies are:

Atlantic Oceanographic and Meteorological Laboratories (AOML): Geology and geophysics of ocean basins and borders, oceanic processes, sea-air interactions and remote sensing of ocean processes and characteristics (Miami, Florida).

Pacific Marine Environmental Laboratory (PMEL): Environmental processes with emphasis on monitoring and predicting the effects of man's activities on estuarine, coastal, and near-shore marine processes (Seattle, Washington).

Great Lakes Environmental Research Laboratory (GLERL): Physical, chemical, and biological, limnology, lake-air interactions, lake hydrology, lake level forecasting, and lake ice studies (Ann Arbor, Michigan).

Atmospheric Physics and Chemistry Laboratory (APCL): Processes of cloud and preciptation physics; chemical composition and nucleating substances in the lower atmosphere; and laboratory and field experiments toward developing feasible methods of weather modification.

Air Resources Laboratories (ARL): Diffusion, transport, and dissipation of atmospheric contaminants; development of methods for prediction and control of atmospheric pollution; geophysical monitoring for climatic change (Silver Spring, Maryland).

Geophysical Fluid Dynamics Laboratory (GFDL): Dynamics and physics of geophysical fluid systems; development of a theoretical basis, through mathematical modeling and computer simulation, for the behavior and properties of the atmosphere and the oceans (Princeton, New Jersey).

National Severe Storms Laboratory (NSSL): Tornadoes, squall lines, thunderstorms, and other severe local convective phenomena directed toward improved methods of prediction and detection (Norman, Oklahoma).

Space Environment Laboratory (SEL): Solar-terrestrial physics, service and technique development in the areas of environmental monitoring and forecasting.

Aeronomy Laboratory (AL): Theoretical, laboratory, rocket, and satellite studies of the physical and chemical processes controlling the ionosphere and exosphere of the earth and other planets, and of the dynamics of their interactions with high-altitude meteorology.

Wave Propagation Laboratory (WPL): Development of new methods for remote sensing of the geophysical environment with special emphasis on optical, microwave and acoustic sensing systems.

Marine EcoSystem Analysis Program Office (MESA): Plans and directs interdisciplinary analyses of the physical, chemical, geological, and biological characteristics of selected coastal regions to assess the potential effects of ocean dumping, municipal and industrial waste discharges, oil pollution, or other activity which may have environmental impact.

Weather Modification Program Office (WMPO): Plans and directs ERL weather modification research activities in precipitation enhancement and severe storms mitigation and operates ERL's research aircraft.

NATIONAL OCEANIC AND ATMOSPHERIC ADMINISTRATION
BOULDER, COLORADO 80302

USCOMM - ERL